

Entry System Options for Human Return from the Moon and Mars

Z. R. Putnam,* R. D. Braun,[†] and R. R. Rohrschneider*
Georgia Institute of Technology, Atlanta, Georgia 30332
and
J. A. Dec[‡]

NASA Langley Research Center, Hampton, Virginia 23681

DOI: 10.2514/1.20351

Earth-entry system options for human return missions from the moon and Mars were analyzed and compared to identify trends among the configurations and trajectory options and to facilitate informed decision-making at the exploration architecture level. Entry system options included ballistic, lifting capsule, biconic, and lifting body configurations with direct-entry and aerocapture trajectories. For each configuration and trajectory option, the thermal environment, deceleration environment, crossrange and downrange performance, and entry corridor were assessed. In addition, the feasibility of a common vehicle for lunar and Mars return was investigated. The results show that a low lift-to-drag ratio ($L/D = 0.3$) vehicle provides sufficient performance for both lunar and Mars return missions while providing the following benefits: excellent packaging efficiency, low structural and thermal protection system mass fraction, ease of launch vehicle integration, and system elegance and simplicity. Numerous configuration options exist that achieve this lift-to-drag ratio.

Nomenclature

C_D	= hypersonic drag coefficient, nondimensional
C_L	= hypersonic lift coefficient, nondimensional
d	= characteristic diameter, m
L	= characteristic length, m
L/D	= lift-to-drag ratio, nondimensional
m	= mass, kg
r_N	= effective nose radius, m
S_{ref}	= aerodynamic reference area, m ²
α	= angle of attack, deg
β	= ballistic coefficient, kg/m ²
γ	= inertial flight-path angle, deg

I. Introduction

THE renewed interest in human exploration beyond low Earth orbit (LEO) has led to many different viewpoints on what exploration architecture is appropriate for human missions to the moon and Mars. Although numerous exploration architectures exist, most require high-speed, aeroassisted deceleration of a crewed vehicle at Earth. There are many possible options for the entry system, and selection among these options will have a significant effect on the overall exploration architecture. The entry system is typically carried through an entire mission and, therefore, its mass, size, and complexity can have a large impact on other architectural elements. This study seeks to compare a broad range of entry system

options for high-speed entry at Earth to facilitate competent selection at the architecture level and to update previous studies of this topic [1–5] by using current technology assumptions.

Entry system selection for future human exploration architectures will likely be based on different criteria than used in design of the only previous such system, the Apollo command module (CM). The design driver for the amount of lift generated by the Apollo CM was navigation error at atmospheric interface: the required lift-to-drag ratio required was 0.25 [1]. Today, significant improvements in Earth approach navigation significantly reduce the lift-to-drag ratio requirements. In addition, the Apollo CM guidance was designed to allow a maximum deceleration of 12 g during nominal entry [2]. Typical Apollo missions reached peak decelerations over 6.5 g during entry [6]. With a long-term focus on human exploration of Mars, lunar mission durations will be significantly longer than the Apollo program to prepare for multiyear missions to Mars [7]. These missions will subject astronauts to micro and low gravity for long periods of time and may require more stringent limits on deceleration during Earth entry than used in the Apollo program to ensure the safe return of physiologically deconditioned astronauts.

Aerocapture guidance was a flight option for the Apollo program, which required a lift-to-drag ratio of 0.25, although it was never used [1]. Studies from the early 1990s of the aerocapture Mars return mission advocate a minimum lift-to-drag requirement of 0.5 [3–5]. However, it was assumed that a large entry corridor (0.5 to 1.0 deg) was necessary for Mars return. The entry corridor is the range of flight-path angles at which the vehicle can enter the atmosphere for a successful aeroassist maneuver. The width of this corridor is specified by the amount of navigation and atmospheric uncertainty that the vehicle must mitigate during atmospheric flight. To satisfy entry trajectory requirements, entry vehicles use lift to mitigate the uncertainty present at atmospheric interface. A lesser amount of lift, and thus a lesser lift-to-drag ratio, is required for smaller corridor widths. Because of the significant improvements in approach navigation demonstrated by the Stardust and Genesis missions [8], future corridor width requirements for Earth return missions will be less stringent, allowing lower lift-to-drag ratio vehicles to be used. Previous studies show that lower lift-to-drag ratio aeroassist vehicles generally result in lower mass and lower cost vehicles [9], making a low lift-to-drag ratio desirable. In addition, the use of a single vehicle for both lunar and Mars return is an attractive option and this study seeks to investigate its feasibility by examining the increase in

Presented as Paper 5915 at the AIAA Atmospheric Flight Mechanics Conference and Exhibit, San Francisco, California, 15–18 August 2005; received 3 October 2005; revision received 15 May 2006; accepted for publication 15 May 2006. Copyright © 2006 by Z. R. Putnam and R. D. Braun. Published by the American Institute of Aeronautics and Astronautics, Inc., with permission. Copies of this paper may be made for personal or internal use, on condition that the copier pay the \$10.00 per-copy fee to the Copyright Clearance Center, Inc., 222 Rosewood Drive, Danvers, MA 01923; include the code \$10.00 in correspondence with the CCC.

*Graduate Research Assistant, School of Aerospace Engineering, 270 Ferst Drive. Student Member AIAA.

[†]Associate Professor, School of Aerospace Engineering, 270 Ferst Drive. Associate Fellow AIAA.

[‡]Thermal Engineer, Structural and Thermal Systems Branch, 1 North Dryden Street, Mail Stop 431.

required lift-to-drag ratio necessary over lunar return requirements to support Mars return missions.

II. Approach

This study uses simulation and other computational methods to analyze the performance of several entry systems options. Uncertainty analyses, including atmospheric, aerodynamic, and vehicle property dispersions, were not performed. However, when possible, conservative assumptions were used.

A. Computational Methods

Historic aerodynamic data was used when available for this analysis. For nonheritage vehicles, aerodynamic analysis was performed using the tangent cone method option in the aerodynamic preliminary analysis system (APAS) [10]. The fidelity of the aerodynamic data in the hypersonic regime generated by APAS was on the order of the fidelity of the trajectory and heat shield sizing analyses performed. Although the accuracy of the APAS analysis was significantly poorer in the subsonic and supersonic regimes, these inaccuracies introduce only small errors in the analyses, as aerodynamics in the hypersonic regime dominate entry vehicle performance.

Trajectory analysis of atmospheric entry at Earth was performed with the three-degree-of-freedom version of the program to optimize simulated trajectories (POST) [11]. Several important features of POST were used, including the parachute drag model and the linear feedback control option. The linear feedback control option was used to fly constant altitude and constant deceleration entry trajectories by using lift control through bank-angle modulation.

Aeroheating calculations were performed with two stagnation-point heating approximation methods. Convective heating was calculated using Chapman's equation [12] and radiative heating was calculated using the Tauber-Sutton approximation for Earth entry [13]. The Tauber-Sutton approximation is valid only for nose radii up to 3 m, requiring this study to approximate nose radii larger than 3 m. The results for both calculations were summed to find the total stagnation-point heat rate and integrated heat load as a function of time for each trajectory.

Forebody heat shield stagnation-point thickness analyses were performed with the charring material thermal response and ablation program (CMA) [14]. CMA is a finite difference computational tool used to compute the 1-D transient thermal response of a 3-D isotropic material that can ablate from the surface and decompose in depth.

B. Nominal Aeroassist Trajectories

This study analyzed two types of aeroassist trajectories: direct entry and aerocapture. Direct entry uses a planetary atmosphere to decelerate the vehicle and land on the planet's surface (Fig. 1a). Direct entry may occur from inbound hyperbolic trajectories or from orbit. Aerocapture uses a planetary atmosphere to decelerate a vehicle on an inbound hyperbolic trajectory. However, during aerocapture, the vehicle exits the atmosphere with the correct orbital energy to enter orbit around the planet (Fig. 1b).

Direct entry is defined to be a trajectory that does not exit the atmosphere once it has reached atmospheric interface. A nominal direct entry begins at atmospheric interface at 122-km (400,000-ft) altitude with a given inertial velocity and flight-path angle (Fig. 2a). Atmospheric effects, including lift and drag, are negligible at this altitude. As the vehicle descends through the atmosphere, dynamic pressure increases quickly, causing hypersonic aerodynamics to dominate the vehicle dynamics. Aerodynamic forces decelerate the vehicle, and the vehicle quickly passes through peak heating and peak deceleration (Figs. 2b and 2c). The magnitudes of sensed deceleration and heat rate can be mitigated through judicious use of lift generated by the vehicle. The constant altitude flight segment in Fig. 2a is an example of this. When the vehicle decelerates to Mach 2, drogue chutes are released to ensure stability in the supersonic regime. Main chutes are deployed at approximately 1-km altitude after the vehicle has reached subsonic velocity (Fig. 2b). The main chutes reduce the vehicle's touchdown velocity to approximately 8 m/s. This touchdown velocity is consistent with the Apollo program, whose splashdown velocity was approximately 31 ft/s (9.44 m/s) [15]. This study does not model the terminal descent or touchdown phase of direct entry.

A nominal aerocapture trajectory also begins at atmospheric interface at 122-km altitude. The vehicle enters the atmosphere and begins to decelerate as drag increases on the vehicle (Fig. 3a). For the purposes of this study, at peak deceleration, the vehicle uses lift control to fly a constant altitude segment in the atmosphere (Fig. 3b). At the proper time, the vehicle switches to a full lift-up orientation to exit the atmosphere with the proper orbital energy (Fig. 3a).

A variety of techniques can be used to mitigate the high heating rates and g loads experienced during direct entry and, to a lesser extent, during aerocapture. This study focused exclusively on lift control through bank-angle modulation. Changes in bank angle are assumed to be achieved propulsively through a reaction control system.

C. Entry Corridor Definition

For a given inertial velocity at atmospheric interface, there are many possible trajectories that satisfy a given set of constraints. Variation within these constraints may be achieved by reorienting the lift vector of the vehicle through bank-angle modulation. For direct entry, if the initial flight-path angle is too shallow, the vehicle will skip out of the atmosphere. If the initial flight-path angle is too steep, the vehicle will not dissipate enough energy before it reaches the surface of the planet. For aerocapture, if the initial flight-path angle is too shallow, not enough energy will be dissipated during the atmospheric pass. If the flight-path angle is too steep, too much energy will be dissipated. The locus of all possible lift-modulated trajectories defined by the two boundaries for direct entry and aerocapture is known as the aerodynamic entry corridor.

In addition to the previously mentioned constraints, additional requirements may be imposed on aeroassist trajectories that define an operational corridor. Such constraints may include limits on the peak heat rate, total integrated heat load, or on the peak deceleration. Peak heat rate and peak deceleration typically limit the steep, or

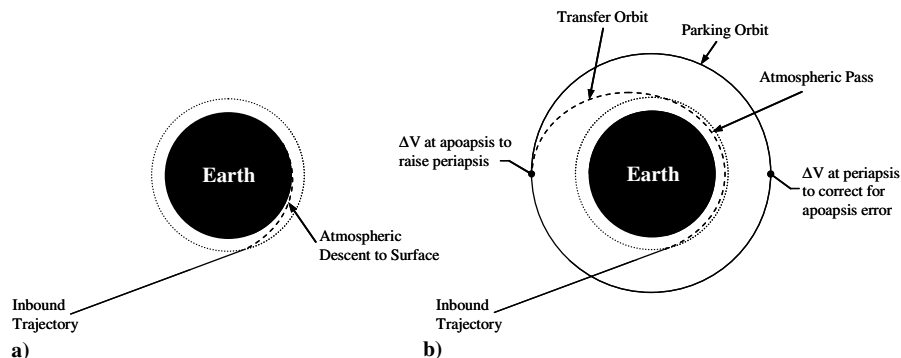


Fig. 1 Aeroassist trajectories: a) direct entry and b) aerocapture.

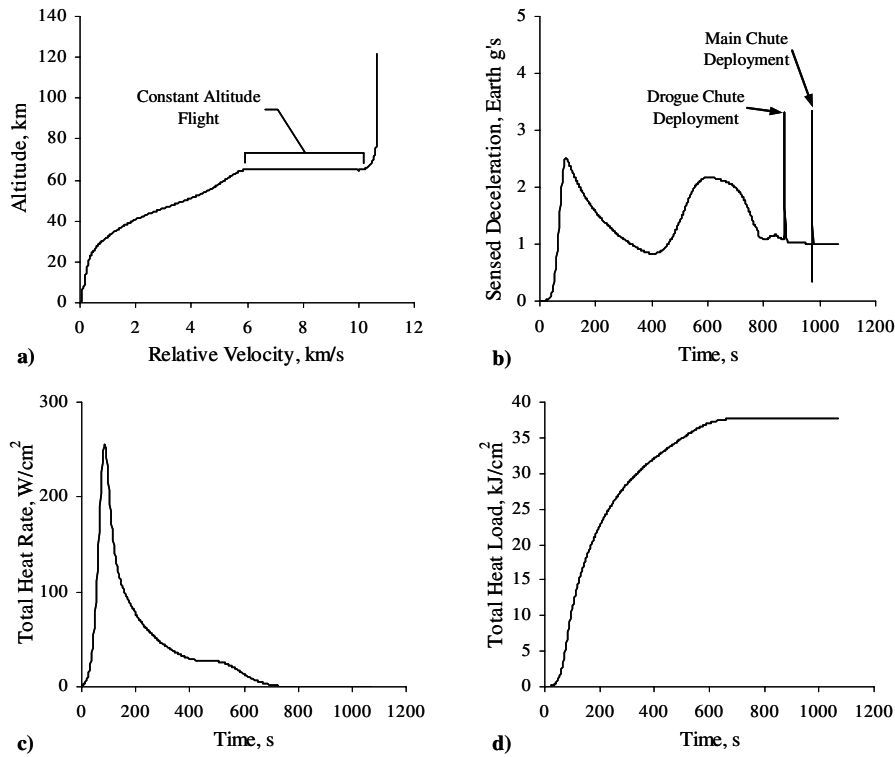


Fig. 2 Nominal lunar return direct-entry trajectory; inertial velocity is 11 km/s, $L/D = 0.3$, $\beta = 365 \text{ kg/m}^2$, $\gamma = -5.61^\circ$, and $r_N = 3.0 \text{ m}$.

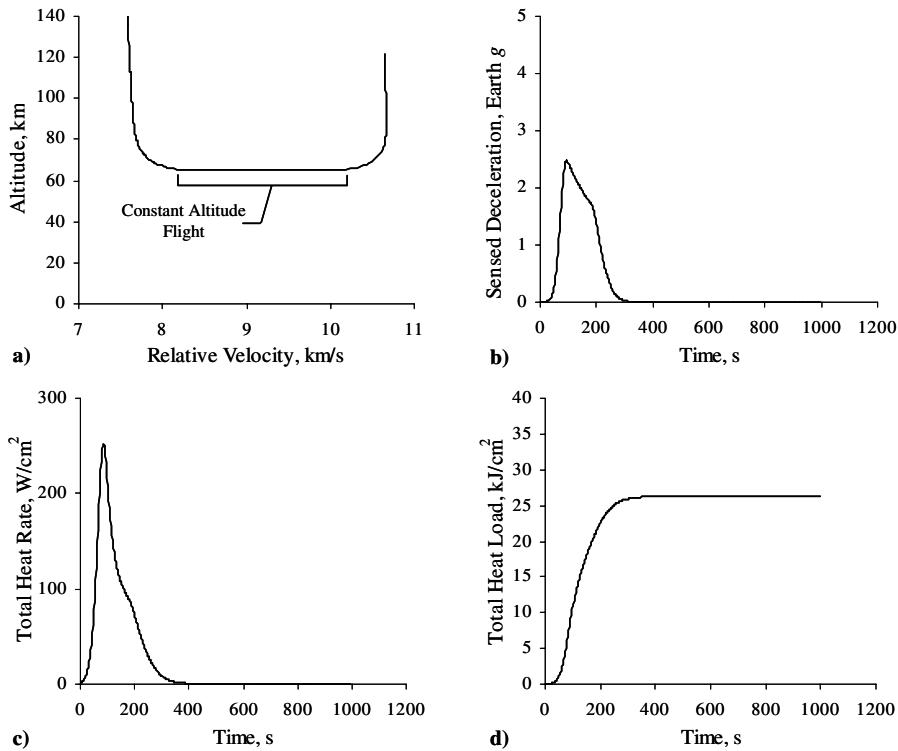


Fig. 3 Nominal lunar return aerocapture trajectory; inertial velocity is 11 km/s, $L/D = 0.3$, $\beta = 365 \text{ kg/m}^2$, $\gamma = -5.61^\circ$, and $r_N = 3.0 \text{ m}$.

undershoot, boundary, whereas limits on the integrated heat load will limit the shallow, or overshoot, boundary [16]. For this study, a peak deceleration limit of 5 Earth g was imposed, limiting the undershoot boundary.

Sample corridors are shown in Figs. 4 and 5 for direct entry and aerocapture. For direct entry, the overshoot boundary is achieved with a lift-down orientation, followed by constant altitude flight to reduce peak deceleration. The aerodynamic undershoot boundary is

achieved with a lift-up orientation and a -90° flight-path angle. Note that this trajectory reaches a peak deceleration in excess of 360 Earth g and represents a vertical dive. The operational undershoot boundary is achieved with a lift-up orientation and constant deceleration flight to limit peak deceleration. For aerocapture, the overshoot boundary is achieved with a lift-down orientation throughout the trajectory. The aerodynamic undershoot boundary of the corridor is achieved with a lift-up orientation. The

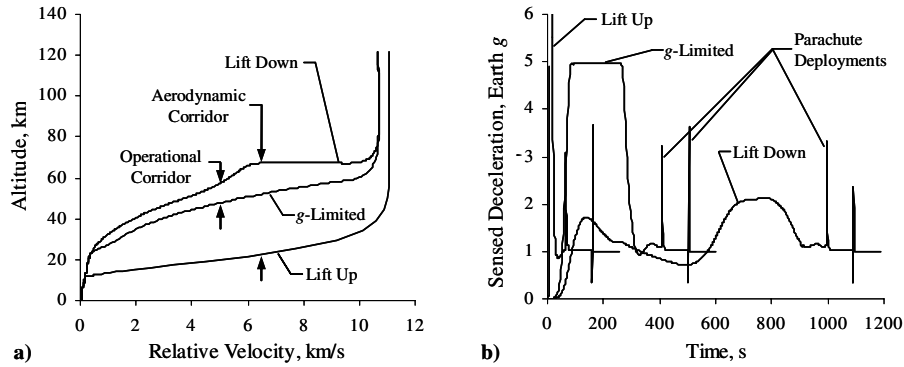


Fig. 4 Sample lunar return direct-entry corridor trajectories; inertial velocity is 11 km/s, $L/D = 0.3$, and $\beta = 365 \text{ kg/m}^2$.

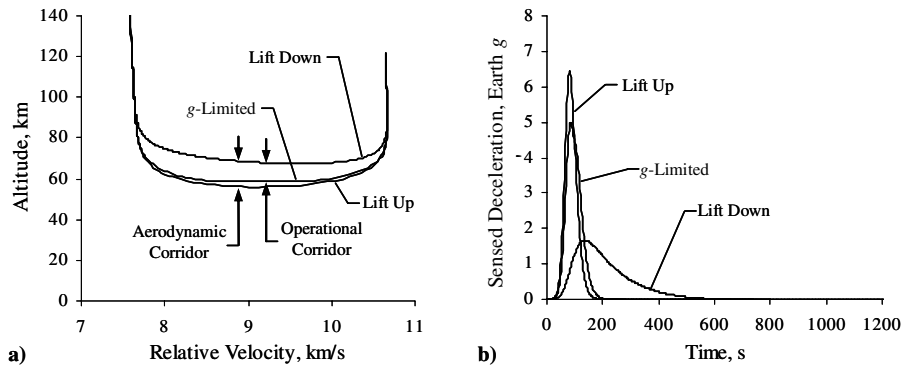


Fig. 5 Sample lunar return aerocapture corridor trajectories; inertial velocity is 11 km/s, $L/D = 0.3$, and $\beta = 365 \text{ kg/m}^2$.

operational corridor is further limited by the peak deceleration limit of 5 g. The undershoot boundary of the operational corridor is achieved with a lift-up orientation followed by bank-angle modulation to achieve the required exit energy.

D. Trajectory Requirements

To facilitate a comparative analysis, deceleration and corridor width requirements were imposed on all trajectories simulated in this study. It should be noted that no requirements were imposed on vehicle angular rates.

1. Peak Deceleration Limit

Although NASA has not specified deceleration requirements for a crewed entry vehicle, it is desirable to limit the peak deceleration for the human crew. Reducing the peak deceleration becomes more important for crews that have been subjected to a low gravity or microgravity environment for an extended period of time, such as on return from extended-duration lunar missions or Mars missions. This study adopted a maximum peak deceleration limit of 5 Earth g, or 45.05 m/s^2 , a value consistent with current literature on human missions to the moon and Mars as well as with Soviet experience with the Soyuz entry vehicle returning crews from extended-duration missions on Mir [17]. No limit was placed on the duration of high-magnitude deceleration.

2. Entry Corridor Width

The flyable entry corridor was defined to be the difference in inertial flight-path angle between the overshoot and undershoot boundaries, subject to the peak deceleration limit. For the purposes of this study, the minimum entry corridor width was assumed to be 0.4 deg. This conservative estimate is derived from recent entry uncertainty analyses used in the Stardust and Genesis sample return missions [18,19]. The uncertainty requirement in the inertial flight-path angle at atmospheric interface for the Stardust and Genesis sample return capsules (SRCs) was ± 0.08 deg. For a crewed mission, additional conservatism is warranted. A corridor width of

0.4 deg, more than double the Stardust and Genesis SRC values, provides significant conservatism, greatly reducing the level of risk in any human exploration architecture entry system.

3. Skipping Trajectories

Lifting direct-entry trajectories often possess regions in which the vehicle regains some altitude in a skipping maneuver. A full range of skipping trajectories exists from small skips of a few kilometers to aerocapture, in which the skip is so large as to be considered a transfer orbit. For the purposes of this study, exoatmospheric skipping trajectories were not considered for direct entry. An exoatmospheric skipping trajectory is a trajectory in which the vehicle enters the atmosphere, skips out to an altitude above atmospheric interface (122 km), and then reenters the atmosphere.

4. Aerocapture Parking Orbits

All aerocapture trajectories captured into a transfer orbit with a semimajor axis of 6640 km, corresponding to an orbital energy of $-30 \text{ km}^2/\text{s}^2$. This transfer orbit allows direct insertion into LEO. Although capturing into higher-energy orbits is possible and reduces the amount of energy that must be dissipated during the atmospheric pass, capturing into LEO offers several benefits for crewed vehicles: LEO orbits do not involve multiple passes through the Van Allen radiation belts and they facilitate rendezvous with the International Space Station and other orbiting infrastructure. Propulsive maneuvers required for orbit circularization and correction after the atmospheric pass were not examined in this study.

E. Vehicle Concepts

A set of vehicle concepts representing a broad range of options was selected for this study. The set includes moldlines with lift-to-drag ratios ranging from 0 to approximately 1.4. The optimum vehicle moldlines for lunar and Mars return missions depends on many factors, including range, deceleration, and aerothermodynamic performance; packaging; complexity; and cost. Each vehicle in the set represents a different balance of these factors. The set of vehicles

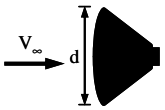
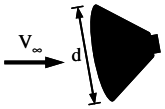
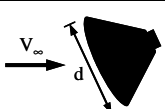
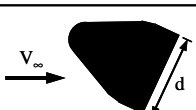
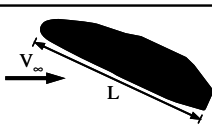
Vehicle Name	Vehicle Moldline	Description
Ballistic Capsule		Hypersonic $L/D = 0.0$ at $\alpha = 0$ deg ($C_L = 0.00$, $C_D = 1.29$) $S_{ref} = 12 \text{ m}^2$, $d = 3.9 \text{ m}$, $r_N = 3 \text{ m}$ Mass: 5500 kg Apollo Command Module aerodynamics.
Low-lift Capsule		Hypersonic $L/D = 0.1$ at $\alpha = -10$ deg ($C_L = 0.13$, $C_D = 1.29$) $S_{ref} = 12 \text{ m}^2$, $d = 3.9 \text{ m}$, $r_N = 3 \text{ m}$ Mass: 5500 kg Apollo Command Module aerodynamics.
Apollo Capsule		Hypersonic $L/D = 0.3$ at $\alpha = -25$ deg ($C_L = 0.39$, $C_D = 1.29$) $S_{ref} = 12 \text{ m}^2$, $d = 3.9 \text{ m}$, $r_N = 3 \text{ m}$ Mass: 5500 kg Apollo Command Module aerodynamics.
Biconic		Hypersonic $L/D = 0.55$ at $\alpha = -25$ deg ($C_L = 0.34$, $C_D = 0.61$) $S_{ref} = 19.6 \text{ m}^2$, $d = 5.0 \text{ m}$, $r_N = 2 \text{ m}$ Mass: 8000 kg Biconic CEV concept from Draper Labs/M.I.T. CE+R study. Aerodynamic data generated in APAS.
Lifting Body		Hypersonic $L/D = 1.4$ at $\alpha = -25$ deg ($C_L = 1.59$, $C_D = 1.16$) $S_{ref} = 5.0 \text{ m}^2$, $L = 9.75 \text{ m}$, $r_N = 2 \text{ m}$ Mass: 8000 kg Simple lifting body CEV concept. Aerodynamic data generated in APAS.

Fig. 6 Vehicle types analyzed.

includes a ballistic capsule, a low-lift capsule, the Apollo CM, an axis-symmetric biconic, and a simple lifting body [20], shown in Fig. 6. All vehicles are designed to carry four crew members. The capsule vehicles use aerodynamic data for the Apollo CM, obtained from [21], and are assumed to have the same nose radii, obtained from [22]. It is assumed that advanced materials allow the capsule vehicles to carry four crew members with masses similar to that of the original Apollo CM. The lifting body and biconic aerodynamic data were obtained from APAS. This study assumes that changes in aerodynamic properties due to forward heat shield ablation were negligible. The nose radii for each vehicle are the effective radii at the hypersonic stagnation point.

The biconic and lifting body vehicles offer the highest lift-to-drag ratios but are more massive and complex. Their poor volumetric efficiency gives rise to increased thermal protection system (TPS) and structural masses. The capsule vehicles offer low complexity and low mass at the expense of lift-to-drag ratio.

An Apollo-style parachute system was used during the terminal descent phase for each of the vehicles. This system consists of two mortar-deployed drogues and three mortar-deployed main parachutes. Nominal velocity at touchdown is approximately 8 m/s. Relevant information for the parachute system is given in Table 1.

F. Parameter Ranges

Planetary entry trades can be largely parameterized across the following four key design variables: atmospheric entry velocity magnitude, atmospheric entry velocity flight-path angle, vehicle ballistic coefficient, and vehicle lift-to-drag ratio.

Inertial velocity at atmospheric interface was varied throughout the study from 7 to 14 km/s. An entry velocity of 7 corresponds to entry from LEO. An entry velocity of 11 km/s corresponds to lunar return. Entry velocities from 11 to 14 km/s represent a range of expected entry velocities across mission opportunities and Mars

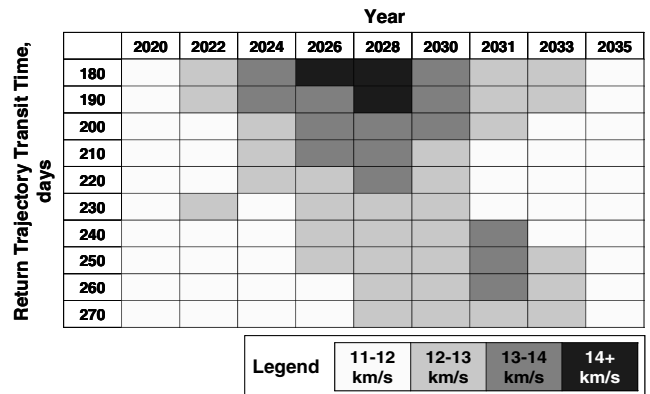


Fig. 7 Inertial Mars return velocity at Earth atmospheric interface as a function of year and transit time.

return transit times, with 14 km/s allowing return durations of 200 days or less in all opportunities, as shown in Fig. 7. All trajectories used the Apollo 11 position vector and heading (see Table 2) at atmospheric interface, with variations in flight-path angle and inertial velocity only.

Although multiple definitions exist for ballistic coefficient, in this study, β was defined as

$$\beta = m/C_D S_{ref}$$

Ballistic coefficient was varied by scaling the mass of a given vehicle. In select analyses, β was varied between 200 and 600 kg/m².

Table 1 Relevant parachute parameters [23]

Parameter	Drogues	Main parachutes
Number of parachutes	2	3
Type	Supersonic drogue	Ringsail
Drag coefficient	0.55	0.85
Inflated diameter	5.0 m	25.4 m

Table 2 Apollo 11 position vector and heading at atmospheric interface

Parameter	Value
Azimuth	50.18 deg
Longitude	171.96° W
Latitude	−3.19° N
Altitude	121,920 m

III. Results and Discussion

A. Direct-Entry Deceleration Performance

Figure 8 shows the hypersonic lift-to-drag ratio required to satisfy a prescribed peak deceleration limit and a 0.4-deg entry corridor width for direct entry. The figure shows that a significant decrease in peak deceleration can be obtained with a small amount of lift. For example, at lunar return speeds (11 km/s), a lift-to-drag ratio of 0.65 reduces the peak deceleration to about 2 g, a significant improvement over the ballistic capsule peak deceleration of 8 g. Note that a lift-to-drag ratio of 0.3 can achieve a 5-g deceleration limit even at very high velocity (14 km/s). With lift-to-drag ratio of 0.4, a 3.5-g limit can be achieved for all but the highest velocities, whereas the lift-to-drag ratio must be increased to 1 or more to reduce the peak deceleration to 2 g. Diminishing peak deceleration reductions with increasing L/D show that the deceleration performance difference between a capsule ($L/D \approx 0.3$ – 0.4) and a lifting body ($L/D \geq 1$) is small. Note that if navigation accuracy were improved beyond the conservative 0.4-deg entry corridor width assumed, an even lower lift-to-drag ratio would be required.

Figure 8 also shows that the peak deceleration for ballistic entry from LEO and lunar return are similar. At hyperbolic entry velocities, the vehicle quickly builds dynamic pressure as atmospheric density increases exponentially with decreasing altitude. This sudden increase in dynamic pressure leads to an increase in drag and causes the trajectory to temporarily shallow out, therefore reducing the peak deceleration beyond what one would expect. If the flight-path angle is too shallow at this point, the vehicle will regain altitude and may skip out of the atmosphere. Ballistic entries from LEO do not produce sufficient dynamic pressure to produce this phenomenon.

B. Direct-Entry Corridor

The entry corridor width was determined for several entry velocities, ballistic coefficients, and vehicle types for direct entry, as shown in Fig. 9. The data show that the most influential parameter in determining corridor width is the vehicle lift-to-drag ratio. The lifting body corridor width is approximately twice that of the lifting capsule, due to its much higher lift-to-drag ratio. In contrast, ballistic coefficient does not have a large effect on corridor width, especially at high entry velocities. As expected, corridor width decreases significantly with increasing entry velocity because of the 5-g deceleration limit. However, it should be noted that both the lifting capsule and the lifting body possesses adequate corridor performance at entry velocities as high as 14 km/s. Although a larger corridor is desirable, it is only desirable from the standpoint that a larger corridor allows greater uncertainty in interplanetary navigation and entry system flight control. However, current robotic missions returning to Earth in this entry velocity range have demonstrated high-accuracy interplanetary navigation techniques that reduce the required corridor width below that assumed in this study. For example, for a corridor width of 0.16 deg, such as that demonstrated by the Stardust and Genesis SRCs, lift-to-drag ratio

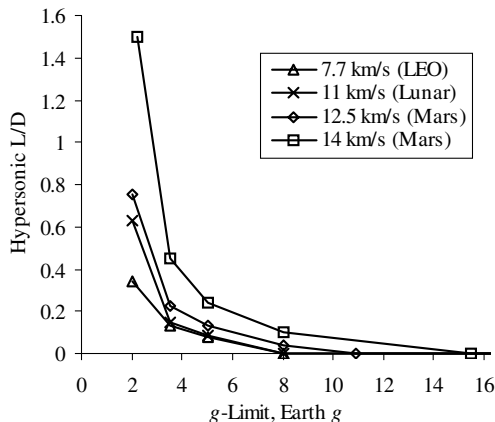


Fig. 8 Required lift-to-drag ratio for direct entry with a given g limit.

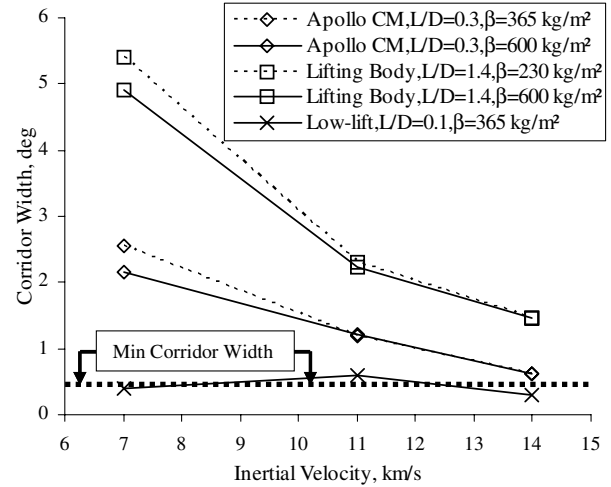


Fig. 9 Direct-entry corridor width for several vehicles.

values less than 0.1 will provide acceptable performance, as shown in Fig. 9.

In conclusion, for a corridor width of 0.4 deg, a lift-to-drag ratio of 0.1 provides sufficient control authority for lunar return speeds. A lift-to-drag ratio of 0.3 provides sufficient control authority with margin for Earth return velocities below 14 km/s.

C. Direct-Entry Range Performance

The range performance of a lifting capsule and a lifting body were compared over several ballistic coefficients for direct-entry trajectories. Range performance was determined subject to the trajectory requirements outlined previously: 5-g deceleration limit, 0.4-deg entry corridor, and no atmospheric skipping. Results are also shown for a skipping capsule to illustrate the range performance of such a trajectory relative to nonskipping trajectories. The primary figures of merit for range performance are the maximum downrange and maximum crossrange capability of a vehicle at a given entry velocity. Downrange is defined as the distance traveled during entry within the orbital plane. Crossrange is defined as the distance traveled perpendicular to the orbital plane. Table 3 shows the range performance for several vehicles at lunar return velocity. Clearly, the range capability of the lifting body was superior. However, the lifting capsule still possesses significant capability, especially if skipping trajectories are employed. This was an option that was flight-certified, but never used, in the Apollo program [2]. Ballistic coefficient has only a small effect on range performance.

Adequate mission design and orbital operations flexibility, in the form of appropriate selection of departure dates and times and judicious use of in-space propulsive capability, provide for minimal downrange and crossrange requirements for lunar and Mars return. In the absence of military operational requirements, such as those dictated for the Space Transportation System (STS) [24], only a modest amount of reach capability necessary for uncertainty mitigation is required for a crewed entry vehicle. This capability is achievable with both capsules and lifting bodies.

D. Direct-Entry Aeroheating

The aeroheating environment dictates the type and size of the TPS required for an entry vehicle. Peak heat rate generally determines the range of possible TPS materials, whereas the integrated heat load determines the thickness and mass of the TPS. Heat rate and integrated heat load calculations were performed with engineering analysis techniques that address both convective and radiative heating contributions.

Figure 10 shows the maximum heat loads and maximum peak heat rates for 5-g-limited direct-entry trajectories. The maximum peak heat load is incurred at the overshoot corridor boundary, whereas the maximum peak heat rate is incurred at the undershoot corridor boundary. The results include both convective and radiative heating.

Table 3 Direct-entry range capabilities at lunar return velocities

Vehicle	Ballistic coefficient, kg/m ²	Downrange capability, km		Crossrange capability, km	
		Minimum	Maximum	Minimum	Maximum
Lifting capsule $L/D = 0.3$	200	1811	5199	0	210
	365	1845	5174	0	209
	600	1870	4573	0	200
Lifting capsule $L/D = 0.3$ skipping trajectory	365	2000	10,000+	0	1000+
Lifting body $L/D = 1.4$	200	2053	19747	0	4509
	400	2095	19910	0	4370
	600	2123	20780	0	4152

For blunt bodies entering at lunar return velocities (11 km/s) and greater, peak stagnation-point heat rates are high, approximately 300 W/cm² for lunar return and 1500 W/cm² for Mars return velocities. However, for lifting bodies, the peak heat rates are even higher, with rates in excess of 4500 W/cm² for some Mars return velocities. These high heat rates are driven by the smaller nose radius of the lifting body and its ability to dive more steeply into the atmosphere while maintaining a 5-g limit.

For the vehicles entering the Earth's atmosphere at speeds above 7 km/s, high heat rates demand an ablative or single-use heat shield. For ablative TPS, high heat loads can translate to a more massive TPS, as TPS thickness and mass may increase with increasing heat loads. Reusable TPS, such as that used by STS, can provide a significant advantage, as the integrated heat load does not have as strong an effect on TPS mass. Figure 11 shows the forebody heat shield thickness as a function of entry velocity for two materials and several vehicles. The two materials are carbon phenolic, a material that can withstand heat rates in excess of 17 kW/cm² but is very massive with a density of approximately 1440 kg/m³, and phenolic impregnated carbon ablator (PICA), a material with a lower heat rate limit but a much lighter weight, with a density of approximately 275 kg/m³. These two materials represent bounding cases for the thickness and mass of the forward heat shield. The stagnation-point TPS thickness was calculated for both materials over a variety of flight entry velocities. The lifting body and biconic vehicles require thicker heat shields due to their high heat loads. Although most of the forebody heat shield will be thinner than the required stagnation-point thickness, the total forebody heat shield mass is a strong function of stagnation-point heat shield thickness. Note that total vehicle TPS mass includes the backshell heat shield and insulation, which will also be larger for lifting and biconic vehicles than for capsules, due to a more intense aeroheating environment and larger backshell TPS acreage.

Some error is introduced in these analyses by the assumption of equal nose radii for the capsule vehicles. This assumption leads to an overprediction of low-lift capsule heating rates at velocities below approximately 12.5 km/s and underprediction at velocities above approximately 12.5 km/s. However, an ablative TPS is required for the low-lift capsule regardless of these errors.

Clearly, a blunt body offers a distinct TPS advantage over a lifting body. Both vehicle types require a nonreusable system for lunar return. A lifting body requires a higher-performance TPS whose thickness and acreage requirements will lead to a more massive system. In contrast, a blunt body can use a lower-performance material with a much lower total TPS mass.

E. Aerocapture Deceleration Performance

Aerocapture trajectories typically exhibit low peak decelerations during the atmospheric pass when compared with direct-entry trajectories, as shown in Fig. 12. For example, to limit deceleration to 5 g at an entry velocity as high as 14 km/s, aerocapture requires a hypersonic lift-to-drag ratio of approximately 0.2. For direct entry, a hypersonic lift-to-drag ratio of about 0.3 is required for the same performance. A lift-to-drag ratio of 0.3 is capable of limiting deceleration to 4 g up to 14 km/s. From Fig. 12, it is readily apparent that increasing the aerocapture vehicle's lift-to-drag ratio beyond 0.3

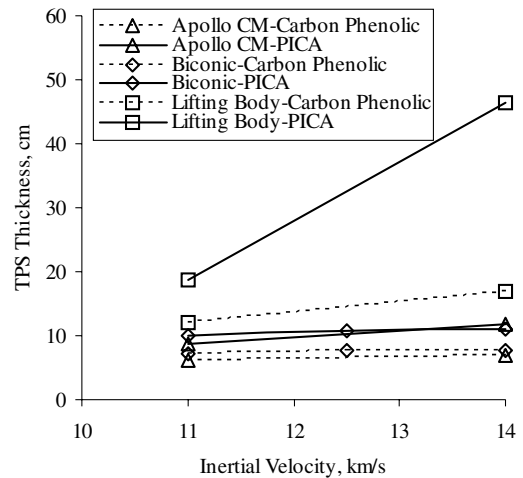


Fig. 11 Direct-entry stagnation-point forebody heat shield thickness for several vehicles.

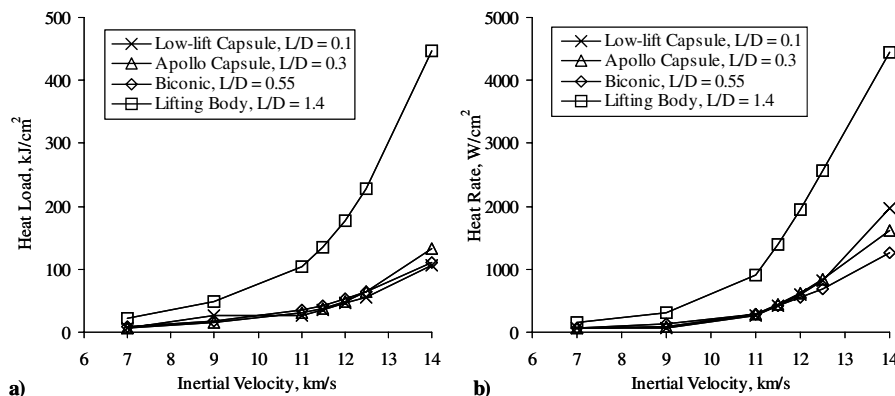


Fig. 10 Direct entry for several vehicles: a) maximum heat load and b) maximum peak heat rate.

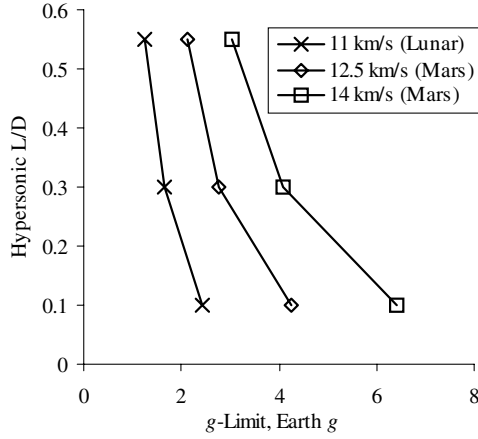


Fig. 12 Aerocapture g limit vs required lift-to-drag ratio.

provides a diminished performance return in performance. The reduction in peak deceleration at 14 km/s is only about 1 g when the lift-to-drag ratio is increased from 0.3 to 0.55. Peak deceleration reduction also decreases with decreasing velocity: the benefit at 11 km/s is only 0.4 g.

F. Aerocapture Corridor

The entry corridor was determined for three different vehicles for aerocapture. Ballistic coefficient was not varied, as it had only a small effect on the direct-entry corridor widths. As for direct entry, aerocapture corridor width decreases as entry velocity increases, due to the imposed 5-g peak deceleration constraint (see Fig. 13). The low-lift capsule ($L/D = 0.1$) provides acceptable performance for velocities lower than about 12 km/s. The Apollo capsule ($L/D = 0.3$) and biconic vehicle ($L/D = 0.55$) provide adequate performance and substantial margin at velocities up to 14 km/s.

The sharp drop in biconic corridor width at high velocity, shown in Fig. 13, is due to the relatively small drag coefficient of this vehicle. At high velocities, the biconic no longer generates enough drag to slow itself at sufficiently high altitude for the overshoot corridor boundary. To increase the drag force on the vehicle and the associated energy dissipation, this vehicle must dive deeper into the atmosphere where the atmospheric density is much higher; however, the 5-g deceleration constraint limits the flyable corridor. Low-altitude deceleration is a primary disadvantage of biconic shapes over blunt bodies for high-speed deceleration: the high lift-to-drag ratios generated by the biconic shape are achieved by reducing the drag coefficient, not increasing the lift coefficient. Although this provides additional control authority during hypersonic flight, it also requires that the vehicle decelerate lower in the atmosphere where the density and resulting peak heat rate and peak deceleration are higher.

Range performance is generally not relevant to the aerocapture mission and was not analyzed.

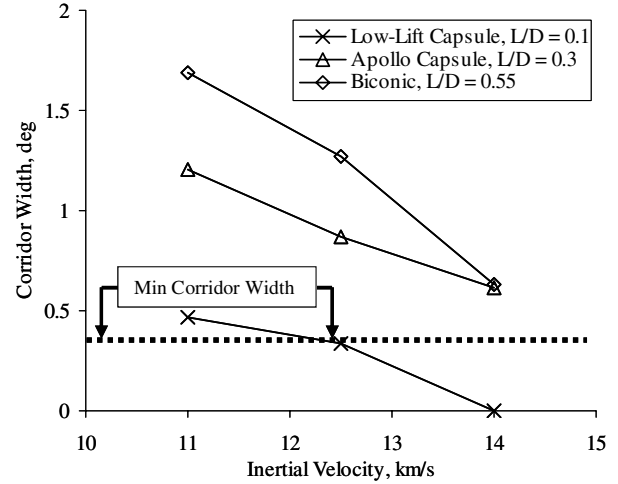


Fig. 13 Aerocapture corridor width for several vehicles.

G. Aerocapture Aeroheating

The aeroheating performance of several vehicles was calculated for nominal aerocapture trajectories. Figure 14 shows the maximum heat loads and maximum peak heat rates for 5-g-limited aerocapture trajectories, with the maximum peak heat load incurred at the overshoot corridor boundary and the maximum peak heat rate incurred at the undershoot corridor boundary. The results include both convective and radiative heating. The maximum peak heat rates for the aerocapture trajectories were nearly equal to those associated with direct entry. The peak heat rate remains unchanged for aerocapture trajectories, because direct entry and aerocapture trajectories are nearly identical before the pull-up maneuver is initiated to exit the atmosphere during aerocapture. It is within this identical trajectory segment that the peak heat rate occurs. Additionally, the maximum total integrated heat loads were slightly less for the aerocapture trajectories. These heating data and comparisons are consistent with previous analyses performed by Lyne et al. in [4].

Similar to the direct-entry data, the aerocapture heating data show that blunt bodies provide superior aeroheating performance, again due to their larger nose radii and high drag coefficients. Also, as expected, the total heat load and peak heat rate increase quickly with velocity at atmospheric interface. High heat rates require ablative TPS for aerocapture at all velocities analyzed.

Again, some error is introduced in these analyses by the assumption of equal nose radii for the capsule vehicles, leading to an overprediction of low-lift capsule heating rates at velocities below approximately 12.5 km/s and underprediction at velocities above approximately 12.5 km/s.

Forebody heat shield thickness was calculated for several vehicles for nominal aerocapture trajectories, shown in Fig. 15. The thicknesses of the aerocapture heat shields are similar to those for direct entry. Again, blunt bodies possess a distinct advantage over higher lift-to-drag ratio vehicles, such as the biconic. Forebody TPS

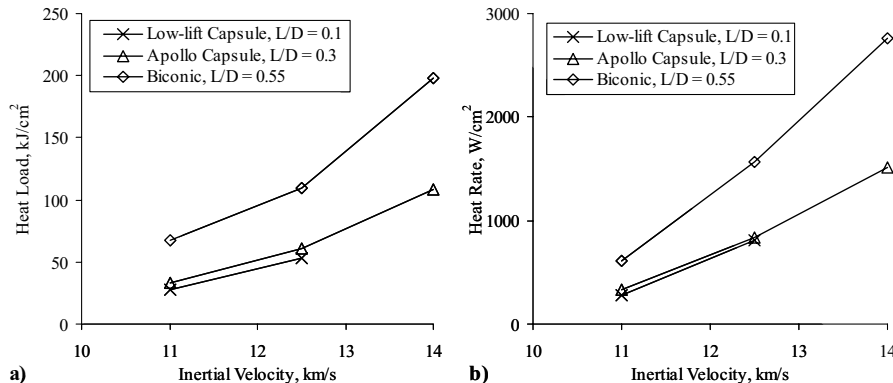


Fig. 14 Aerocapture for several vehicles: a) maximum heat load and b) maximum peak heat rate.

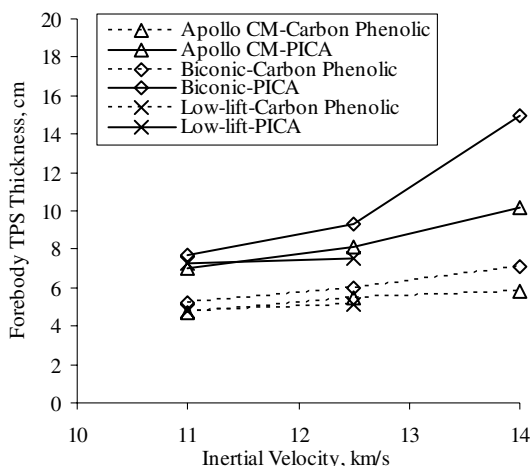


Fig. 15 Aerocapture stagnation-point forebody heat shield thickness for several vehicles.

thicknesses of the biconic are slightly higher than that of the Apollo capsule and low-lift capsule for both PICA and carbon phenolic, due to the biconic's high integrated-heat load. However, the biconic vehicle's overall TPS mass will likely be much larger than that of the Apollo and low-lift capsules, due to the large acreage the biconic's TPS must cover. The inclusion of backshell TPS will likely further increase the TPS mass disparity between the capsules and the biconic.

IV. Conclusion

The performance capabilities of several Earth-entry systems and trajectory options for human return from the moon and Mars have been analyzed and compared. All vehicles considered, with exception of the ballistic vehicles, provide sufficient corridor width and deceleration performance for the lunar return mission for direct entry or aerocapture. Vehicles with lift-to-drag ratios greater than 0.2 provide acceptable performance for the Mars return mission for direct entry or aerocapture. It has been shown that high lift-to-drag ratio vehicles, such as a lifting body ($L/D = 1.4$), offer limited landing site access advantages over moderate lift-to-drag ratio capsules ($L/D = 0.3$). In contrast, moderate lift-to-drag capsules offer significant aerotherm and TPS advantages. The primary consideration for a lifting body vehicle is crossrange performance. Without a significant crossrange requirement (as provided by the U.S. Air Force in development of STS), a capsule vehicle configuration that generates a lift-to-drag ratio of 0.3 is not only sufficient, but provides significant mass, complexity, and risk advantages. This lower lift-to-drag ratio requirement is in contrast to greater lift-to-drag ratio requirements reported in previous analyses. The prime cause of this reduction in required lift-to-drag ratio is improved navigation uncertainty at atmospheric interface.

In addition, it was found that aerocapture trajectories provide limited benefits over direct-entry trajectories. The benefits of an aerocapture trajectory include the ability to rendezvous with orbital assets, simplification of the return targeting problem, and weather uncertainty mitigation. However, rendezvous with orbital assets adds significant complexity and risk to a return mission, the targeting problem is easily solvable with modern navigation techniques, and all vehicles analyzed possess enough downrange capability to abort to an alternate landing site to avoid foul weather at the primary landing site. Therefore, in the absence of requirements that specify aerocapture for operational reasons, direct entry provides adequate performance with reduced complexity and risk.

In conclusion, a lifting capsule Earth-entry system with a lift-to-drag ratio of 0.3 offers sufficient performance for Earth return from the moon and Mars, while providing the following benefits: excellent packaging efficiency, low structural and TPS mass fraction, ease of launch vehicle integration, and system elegance and simplicity. Numerous configuration options exist that achieve this lift-to-drag ratio.

Acknowledgments

This study was conducted under a partnership with the Charles Stark Draper Laboratory as part of the NASA Exploration Systems Mission Directorate Concept Exploration and Refinement study. The guidance and constructive comments of Gregg Barton (Charles Stark Draper Laboratory) and Paul Wooster (Massachusetts Institute of Technology) are appreciated.

References

- [1] Harpold, Jon C., "Minimum Lift-to-Drag Ratio Requirement for the Lunar Mission," NASA TM-X-69752, Oct. 1967.
- [2] Tolin, J. W., Harpold, J. C., and Rogers, J. E., "AS-503A/AS-504A Requirements for the RTCC: Reentry Phase," NASA TM-X-69753, 1967.
- [3] Tauber, M. E., Palmer, G. E., and Yang, L., "Earth Atmospheric Entry Studies for Manned Mars Missions," *Journal of Thermophysics and Heat Transfer*, Vol. 6, No. 2, 1992, pp. 193–199.
- [4] Lyne, J. Evans, Tauber, M. E., and Braun, Robert D., "Parametric Study of Manned Aerocapture Part 1: Earth Return from Mars," *Journal of Spacecraft and Rockets*, Vol. 29, No. 6, 1992, pp. 808–813.
- [5] Braun, R. D., Powell, R. W., and Lyne, J. E., "Earth Aerobraking Strategies for Manned Return from Mars," *Journal of Spacecraft and Rockets*, Vol. 29, No. 3, 1992, pp. 297–304.
- [6] Anon., "Apollo 11 Mission Report," U.S. Manned Spacecraft Center Mission Evaluation Team, Scientific and Technical Information Office, NASA TM-X-62633, 1971.
- [7] Anon., "Exploration Systems Architecture Study Final Report," NASA TM-2005-214062, Nov. 2005.
- [8] Desai, Prasun N., and Lyons, Dan T., "Entry, Descent, and Landing Operations Analysis for the Genesis Re-Entry Capsule," American Astronautical Society Paper 05-121, 2005.
- [9] Walburg, G. D., "A Survey of Aeroassisted Orbit Transfer," *Journal of Spacecraft and Rockets*, Vol. 22, No. 1, 1985, pp. 3–18.
- [10] Sova, G., and Divan, P., "Aerodynamics Preliminary Analysis System 2, Part 2: User's Manual," NASA CR 182077, Apr. 1991.
- [11] Brauer, G. L., Cornick, D. E., and Stevenson, R., "Capabilities and Applications of the Program to Optimize Simulated Trajectories (POST)," NASA CR-2770, Feb. 1977.
- [12] Chapman, D. R., "An Approximate Analytical Method for Studying Entry into Planetary Atmospheres," NACA TN-4276, 1958.
- [13] Tauber, M. E., and Sutton, K., "Stagnation-Point Radiative Heating Relations for Earth and Mars Entries," *Journal of Spacecraft and Rockets*, Vol. 28, No. 2, 1991, pp. 40–42.
- [14] Dec, J. A., and Braun, R. D., "An Approximate Ablative Thermal Protection System Sizing Tool for Entry System Design," AIAA Paper 2006-0500, 2006.
- [15] Anon., "Apollo 11 Lunar Landing Mission Press Kit," NASA News Release 69-83K, 1969, pp. 57–64, 90.
- [16] Chapman, D. R., "An Analysis of the Corridor and Guidance Requirements for Supercircular Entry into Planetary Atmospheres," NASA TR R-55, 1959.
- [17] Lyne, Evans J., "Physiologically Constrained Aerocapture for Manned Mars Missions," NASA TM 103954, Aug. 1992.
- [18] Desai, Prasun N., Mitcheltree, Robert A., and Cheatwood, F. McNeil, "Entry Dispersion Analysis for the Stardust Comet Sample Return Capsule," *Journal of Spacecraft and Rockets*, Vol. 36, No. 3, 1999, pp. 463–469.
- [19] Desai, Prasun N., and Cheatwood, F. McNeil, "Entry Dispersion Analysis for the Genesis Sample Return Capsule," American Astronautical Society Paper 99-469, Aug. 1999.
- [20] Hutchinson, V., Olds, J., Alemany, K., Christian, C., Clark, I., Crowley, J., Krevor, Z., Rohrschneider, R., Thompson, R., Young, D., and Young, J., "Tempest: Crew Exploration Vehicle Concept," AIAA Paper 2005-4190, 2005.
- [21] Graves, C. A., and Harpole, J. C., "Apollo Experience Report: Mission Planning for Apollo Entry," NASA TN D-6727, 1972.
- [22] Ried, R. C., Rochelle, W. C., and Milhoan, J. D., "Radiative Heating to the Apollo Command Module: Engineering Prediction and Flight Measurement," NASA TM X-58091, Apr. 1972.
- [23] Knacke, T. W., *Parachute Recovery Systems Design Manual*, Para Publishing, Santa Barbara, CA, 1992, p. 5-4.
- [24] Heppenheimer, T. A., *The Space Shuttle Decision, 1965–1972*, Smithsonian Inst. Press, Washington, D.C., 2002, pp. 215–217.